Acta Acustica united with Acustica
Vol. 102 (2016) 705 – 713

DOI 10.3813/AAA.918987

On the Modeling of an Emitting Cylindrical Transducer With a Piezoelectric Polymer Membrane

Thomas Lavergne[1)], Zdeněk Škvor[1)†], Libor Husník[1)], Michel Bruneau[2)]

[1)] Faculty of electrical engineering, K13137 Department of Radio engineering, Technická 2, 166 27 Praha 6, Prague, Czech Republic. t.lavergne@gmail.com

[2)] Laboratoire d'Acoustique de l'Université du Maine, Avenue Olivier Messiaen 72085 Le Mans Cedex 9.

Summary

This work aims at providing a theoretical description of an ultrasonic emitting transducer, which consists of a cylindrical Polyvinylidene fluoride (PVDF) membrane coupled to an air-filled back-cavity. Based on the fundamental equations of piezoelectricity and linear acoustics, and assuming axisymmetrical geometry, an analytical model which describes the coupling of the displacement field of the membrane with the pressure fields on both of its sides is presented. Solutions are obtained using modal expansion theory for the displacement field of the membrane and for the acoustic pressure field in the axial-direction of the back-cavity. This model permits to predict the resonances of the system, which are not taken into account in an earlier work [1]. A lumped elements network is then derived from the analytical solution, valid in the lowest frequency range, when keeping only one mode and when considering two levels of approximations. Comparison between measurement results and theoretical ones of the pressure radiated by two prototypes of emitter shows an overall good agreement.

PACS no. 43.38.Fx

1. Introduction

Since the discovery by Heiji Kawai in 1969 [2] of the strong piezoelectric effect in Polyvinylidene fluoride (PVDF), this material has turned out to be useful in many fields of applications, such as acoustical, mechanical and optical devices, electrical components, energy conversion, medical instruments, etc. (lists of applications and patents are provided in [3, 4]). For acoustic transducers, one of the most interesting properties of PVDF films is that, when coated with metallized electrodes, it acts as both a membrane and a direct electromechanical conversion element. The conversion being reciprocal, such films can be used either as part of acoustic sensors [5, 6, 7, 8, 9, 10, 4, 11, 12, 13, 14, 15], as well as part of acoustic actuators [5, 16, 17, 18, 19, 12, 20, 21, 22, 23, 1, 24, 25, 26, 27], or both as transmitter and receiver in a single device [24]. These acoustic transducers described in the literature are mostly based on the excitation of the flexural modes using the transverse piezolectric effect. This effect is illustrated in Figure 1, where an electrical voltage V_r is applied between the electrodes of a PVDF membrane for two different arrangements: when the PVDF membrane has a plane shape (Figure 1a) the coupling to the surrounding medium is weak, whereas when it has a curved shape (Figure 1b) the coupling to the surrounding medium is stronger and the transverse motion is converted into an oscillating displacement field [28].

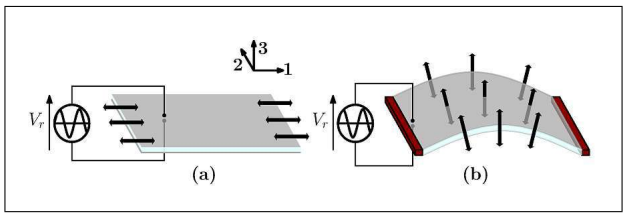

Figure 1. Movement of a PVDF film (adapted from [28]). (a) Plane shaped membrane ; (b) Curve shaped membrane fixed on a rigid support.

Simple designs of transmitters based on this principle include, for example, corrugated film [23, 24], a dome shaped membrane [7, 18, 19, 25], as well as a conical [21, 26] or a cylindrical [5, 16, 17, 10, 12, 20, 21, 1, 27, 29] membrane. The design investigated here, similar to the one presented in [1] and [30], is suitable to be used as part of an ultrasonic ranging sensor [12, 1, 26] [31, Chap. 9.4]. It consists of a quasi 360° cylindrical transmitter with a PVDF membrane set on a rigid support at its circular edges, which is loaded by a rear toroidal air-filled cavity on one side, and loaded by an infinite air-medium on the other side. This kind of cylindrical transducer has the peculiarity of having a quasi omnidirectional horizontal

Received 25 February 2015,
accepted 10 May 2016.

† Died at age 80 in March 2015 in Praha (Czech Republic)

directivity pattern (acoustic pressure as a function of azimuth) [1, 32]. In [1], the author proposes a model, based on a simple design theory, which is sufficient to assess the acoustic pressure radiated by the transmitter, unless resonances due to the intricate mechano-acoustic behavior of the system appear in the frequency band of interest. This is simply due to the fact that only the resonance due to the breathing mode of the membrane is taken into account, and especially because the modal field which takes place in the rear cavity is not considered (a small cavity represented by its acoustic equivalent stiffness is assumed instead). The model presented here aims at taking into account these resonances, in both the radial and the axial directions, which result from the coupling between the displacement of the membrane and the pressure fields on both of its sides. Such model is based on the fundamental equations of the piezoelectricity and the fundamental laws of linear acoustics for a homogeneous fluid at rest. Damping is taken into account in the model. On one hand, the mechanical loss factor of the PVDF membrane is introduced by means of complex stiffness constants [14], and, on the other hand, the effect of both the viscous and thermal boundary layers is taken into account by means of mixed boundary conditions. Solutions to the problem are obtained using modal expansion on the Dirichlet-like modes of the membrane. An electrical equivalent network of the emitting transducer is also provided. It is derived from the solutions when considering only one mode and low frequency approximations. Experimental and theoretical results are then compared.

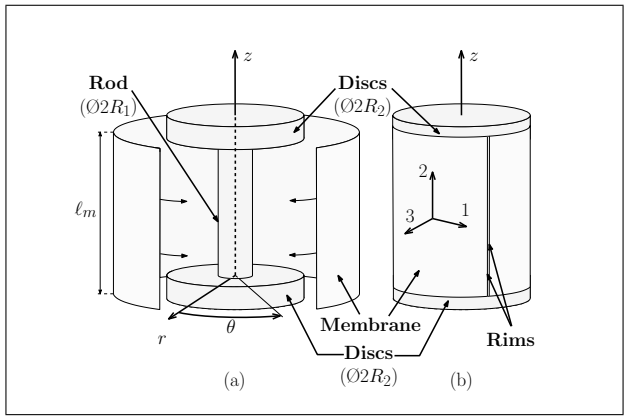

Figure 2. 3D view of the emitting transducer: (a) before fixing the PVDF membrane to the discs, (b) final assembly.

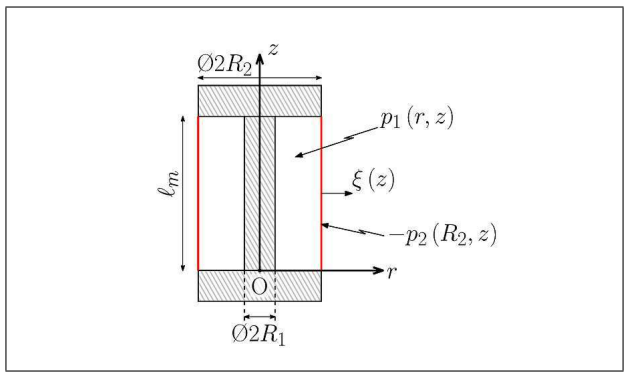

Figure 3. Cross sectional view of the transducer.

2. Analytical model of the transducer

The design of the emitting transducer is shown in Figure 2. It consists of a mono-axially oriented polyvinylidene fluoride (PVDF) membrane of height ℓ_m and thickness t_m, cylindrically curved, fixed at its upper and lower sides. The membrane is wrapped around and fixed using adhesive tape to two discs of radius R_2, which are attached together with a cylindrical rod of radius R_1 and length ℓ_m. Figure 2a shows the cylindrical coordinate system (r, θ, z), which has its origin O at the bottom center of the rod, and whose Oz-axis is parallel to the membrane. Figure 2b shows the orientation of the piezoelectrical axis of the mono-axially oriented PVDF membrane, where, in the cylindrical coordinate system, the principal directions 1, 2 and 3 correspond to the azimuthal direction θ, the axial direction z, and the radial direction r respectively.

As shown in the final assembly presented in Figure 2b, the transducer is not perfectly cylindrically uniform, because the membrane rims are bonded together using adhesive tape, making an inactive part. This part of the membrane is neglected here, assuming that the transducer is axisymmetrical. The electrical voltage of amplitude V_r, applied between the two metallized faces of the membrane, is associated with a uniform electrical field of complex magnitude $E_r = V_r/t_m$ along the r-axis.

The variables used in the modeling hereafter are represented in Figure 3, showing the cross-section of the cylindrical transducer. Note that only the complex amplitudes of variables are considered hereafter, i.e. the term $e^{i\omega t}$ is omitted, where $\omega = 2\pi f$ is the angular frequency, f the frequency, and t the time variable. The system consists of three coupled domains. The first one is the cylindrical membrane, which vibrates in the radial direction and whose complex amplitude ξ depends only on the axial coordinate z. The two others are fluid domains. On one hand, there is the internal toroidal cavity bounded by the cylindrical rod, the two discs, and the membrane ($R_1 < r < R_2$ and $0 < z < \ell_m$), wherein the complex amplitude p_1 of the acoustic pressure depends on both the axial coordinate z and the radial coordinate r. On the other hand there is the infinite free-field space ($r \geq R_2$) for which the comp lex amplitude of the acoustic pressure in the front side of the membrane is denoted p_2.

2.1. Displacement field of the PVDF membrane

Writing the fundamental equations of piezoelectricity for the dynamic strains $S_{\theta\theta}$ and S_{zz} in angular direction 1 and axial direction 2 respectively ($S_{rr} = 0$) leads straightforwardly to

$$S_{\theta\theta} = S_{11} = s_{11}^{E^*} T_{\theta\theta} + s_{12}^{E^*} T_{zz} + d_{31} E_r, \quad (1)$$

$$S_{zz} = S_{22} = s_{21}^{E^*} T_{\theta\theta} + s_{22}^{E^*} T_{zz} + d_{32} E_r, \quad (2)$$

where $T_{\theta\theta}$ and T_{zz} are the dynamic stress in angular direction 1 and axial direction 2 respectively, d_{31} and d_{32}

the piezoelectric coefficients, and $s_{11}^{E^*} = s_{22}^{E^*} = s_{11}^{E}[1 + \mathrm{i}\tan(\delta_m)]$ and $s_{12}^{E^*} = s_{21}^{E^*} = s_{12}^{E}[1 + \mathrm{i}\tan(\delta_m)]$ the complex compliance coefficients of the membrane, where s_{11}^{E} and s_{12}^{E} are the real (or purely) compliance coefficients and $tan(\delta_m)$ the mechanical damping coefficient [14].

In expressing $T_{\theta\theta}$ from Equations (1)–(2) with $S_{zz} = 0$ (to the first order approximation) and $S_{\theta\theta} = \xi(z)/R_2$, and in writing the equilibrium equation of linear elasticity (here reduced to $T_{\theta\theta}/R_2 = f_i$, where f_i are the forces per unit volume acting on the piezoelectric material) leads to

$$\frac{s_{11}^{E^*}}{s_{E^*}}\frac{\xi(z)}{R_2^2} + \frac{s_{12}^{E^*}d_{32} - s_{11}^{E^*}d_{31}}{s_{E^*}R_2}E_r = \\ -\rho_m\frac{\partial^2\xi(z)}{\partial t^2} + \frac{\partial}{\partial z}\frac{F_z^0}{2\pi R_2 t_m}\frac{\partial\xi(z)}{\partial z} - \frac{p_2 - p_1(R_2, z)}{t_m}, \quad (3)$$

where $s_{E^*} = (s_{11}^{E^*})^2 - (s_{12}^{E^*})^2$, and ρ_m being the density of the membrane. On the right hand side of Equation (3), the first term represents the inertia of the membrane, the second term represents the tension due to the force F_z^0 applied along the z-direction, and the third term represents the pressure gradient applied on the membrane. Then, in writing the complex amplitude p_2 as the product of the radiation impedance Z_{rad} and the volume velocity $i\omega\xi(\theta, z)S_2$ of the membrane[33, 25] (where $S_2 = 2\pi R_2\ell_m$ is the surface of the membrane), and using the following notations for the equivalent pressure p_u due to the electric voltage V_r,

$$p_u = \frac{s_{11}^{E^*}d_{31} - s_{12}^{E^*}d_{32}}{s_{E^*}R_2}V_r, \quad (4)$$

and for the tension of the membrane along the z-axis (which is close to zero),

$$T_z = \frac{F_z^0}{2\pi R_2}, \quad (5)$$

leads to the following form of the equation of motion of the membrane:

$$T_z\left(\frac{\partial^2}{\partial z^2} + K^2\right)\xi(z) = -\left[p_1(R_2, z) + p_u\right], \quad (6)$$

with

$$K^2 = \frac{\rho_m t_m\omega^2 - s_{11}^{E^*}t_m/s_{E^*}(R_2)^2 - \mathrm{i}\omega Z_{\mathrm{rad}}S_2}{T_z}, \quad (7)$$

the displacement field of the membrane being subjected to the Dirichlet boundary condition

$$\xi(z = 0) = \xi(z = \ell_m) = 0. \quad (8)$$

Note that the radiation impedance is here approximated by the acoustic radiation impedance of an infinite cylinder such as

$$Z_{\mathrm{rad}} = \frac{\mathrm{i}\rho_0 c_0}{S_2}\frac{H_0^{(2)}(k_0R_2)}{H_1^{(2)}(k_0R_2)}, \quad (9)$$

with $k_0 = \omega/c_0$, and where ρ_0 and c_0 are the density of the gas and the adiabatic speed of sound respectively, $H_0^{(2)}$ and $H_1^{(2)}$ being Hankel functions of the second kind of order zero and one respectively.

The solution of the set of equations (6)–(8) for the displacement field $\xi(z)$ is expressed as an expansion on the eigenfunctions $\psi_\mu(z)$ as

$$\xi(z) = \sum_\mu \xi_\mu\psi_\mu(z), \quad (10)$$

with the odd integer ($\mu = 1, 3, \dots$) labelling the vibration modes along the z-axis, where the eigenfunctions $\psi_\mu(z)$ and their associated eigenvalues k_{z_μ} are given by

$$\psi_\mu(z) = \sqrt{\frac{2}{\ell_m}}\sin\left(k_{z_\mu}z\right), \quad (11)$$

where

$$k_{z_\mu} = \frac{\mu\pi}{\ell_m}, \quad (12)$$

and with

$$\xi_\mu = \frac{-1}{T_z\left[K^2 - \left(k_{z_\mu}\right)^2\right]} \cdot \int_0^{\ell_m}\left[p_1(R_2, z) + p_u\right]\psi_\mu(z)\,\mathrm{d}z. \quad (13)$$

2.2. Pressure field in the internal toroidal cavity

Considering harmonic oscillations of angular frequency ω, the fundamental laws of linear acoustics for a homogeneous fluid at rest without dissipation, outside the sources, lead to the Helmholtz equation,

$$\left(\frac{\partial^2}{\partial r^2} + \frac{1}{r}\frac{\partial}{\partial r} + \frac{\partial^2}{\partial z^2} + k_0^2\right)p_1(r, z) = 0, \quad (14)$$

which is associated with the following boundary conditions:

- at $z = 0$, the admittance-like boundary condition is:

$$\frac{v_{1_z}(r, 0)}{p_1(r, 0)} = \frac{-1}{\mathrm{i}\omega\rho_0}\frac{\partial p_1(r, 0)}{\partial z}\frac{1}{p_1(r, 0)} = Y_{z_q}, \quad (15)$$

where v_{1_z} is the axial component of the particle velocity, and where the specific admittance of the thermo-viscous boundary layers is [34, Chapter 3] (the expression within brackets represents the radial component of the normalized particle velocity)

$$Y_{z_q} = \frac{1}{\rho_0 c_0}\frac{1+\mathrm{i}}{\sqrt{2}}\sqrt{\omega/c_0} \cdot\left\{\left[1 - \left(\frac{q\pi/\ell_m}{k_0}\right)^2\right]\sqrt{\ell_v'} + (\gamma - 1)\sqrt{\ell_h}\right\}, \quad (16)$$

the even integer ($q = 0, 2, \dots$) labelling the acoustic modes along the z-axis (see below Equation 21), $\ell_h =$

$\mu_s/(\rho_0 c_0)$ ($\cong$ 6.12 10^{-8} m) and $\ell'_v = \lambda_h/(\rho_0 c_0 c_p)$ ($\cong$ 4.45 10^{-8} m) being, respectively, the thermal and viscous characteristic lengths for air (under atmospheric pressure at 23°C and 50% of humidity), and where μ_s, λ_h and c_p are the shear viscosity, the thermal conductivity and the heat capacity per unit mass at constant pressure of the fluid respectively;

- at $z = \ell_m$:

$$\frac{v_{1_z}(r, \ell_m)}{p_1(r, \ell_m)} = \frac{1}{\mathrm{i}\omega\rho_0} \frac{\partial p_1(r, \ell_m)}{\partial z} \frac{1}{p_1(r, \ell_m)} = Y_{z_q}; \quad (17)$$

- at $r = R_1$, the admittance-like boundary condition on the central rod is:

$$\frac{v_{1_r}(R_1, z)}{p_1(R_1, z)} = \frac{-1}{\mathrm{i}\omega\rho_0} \frac{\partial p_1(R_1, z)}{\partial r} \frac{1}{p_1(R_1, z)} = Y_{r_q}, \quad (18)$$

where v_{1_r} is the radial component of the particle velocity, and where the specific admittance of the thermo-viscous boundary layers is given by [34, Chapter 3] (the expression within brackets represents the axial component of the normalized particle velocity)

$$Y_{r_q} = \frac{1}{\rho_0 c_0} \frac{1+\mathrm{i}}{\sqrt{2}} \sqrt{\omega/c_0} \cdot \left\{ \left(\frac{q\pi/\ell_m}{k_0} \right)^2 \sqrt{\ell'_v} + (\gamma - 1)\sqrt{\ell_h} \right\}; \quad (19)$$

- at $r = R_2$, the velocity $i\omega\xi(z)$ of the membrane is taken into account as well as the effect of the thermo-viscous boundary layers, leading to the following mixed-boundary condition:

$$\frac{\partial}{\partial r} p_1(r = R_2, z) + \mathrm{i}\omega\rho_0 Y_{r_q} p_1(r = R_2, z) = \omega^2 \rho_0 \xi(z). \quad (20)$$

The solution to Equation (14) for the acoustic pressure in the cavity, symmetrical with respect to $z = \ell_m/2$ and satisfying the boundary conditions (15) and (17), can be expressed as a modal expansion (with respect to the z-coordinate) as

$$p_1(r, z) = \sum_{q=0,2,4,\ldots}^{\infty} A_q \nu_q \cos\left[k_{p_q}(z - \ell_m/2)\right] \cdot \left[J_0(\chi_q r) + B_q N_0(\chi_q r)\right], \quad (21)$$

where J_0 and N_0 are Bessel functions of order zero and of the first kind and the second kind respectively, and with

$$\nu_q = \begin{cases} \sqrt{1/\ell_m}, & \text{if } q = 0, \\ \sqrt{2/\ell_m}, & \text{otherwise,} \end{cases} \quad (22)$$

$$\chi_q = \sqrt{k_0^2 - k_{p_q}^2}, \quad (23)$$

the eigenvalues k_{p_q} being given by

$$k_{p_q} \cong \begin{cases} \epsilon_0, & \text{if } q = 0, \\ q\pi/\ell_m + \epsilon_q, & \text{otherwise,} \end{cases} \quad (24)$$

with

$$\epsilon_q = \begin{cases} \sqrt{2i\omega\rho_0 Y_{z_0}/\ell_m}, & \text{if } q = 0, \\ 2i\omega\rho_0 Y_{z_q}/(q\pi), & \text{otherwise.} \end{cases} \quad (25)$$

Note that the evanescent modes for which $[(k_0)^2 < k_{p_q}^2]$ are not taken into account in the calculation. Then, the expression of constant B_q is determined from the admittance-like boundary condition (18), leading to

$$B_q = -\frac{J_1(\chi_q R_1) + \mathrm{i}\omega\frac{\rho_0}{\chi_q} Y_{r_q} J_0(\chi_q R_1)}{N_1(\chi_q R_1) + \mathrm{i}\omega\frac{\rho_0}{\chi_q} Y_{r_q} N_0(\chi_q R_1)}, \quad (26)$$

and the constant A_q, determined from the mixed-boundary condition (20) is given by

$$A_q = \sum_{\mu=1,3,\ldots}^{\infty} \left\{ \left[-\omega^2 \rho_0 \sqrt{\frac{2}{\ell_m}} \nu_\mu \frac{\mu \ell_m}{\pi} \cdot \left[\cos\left(\frac{q\pi}{2} + \frac{\epsilon_q \ell_m}{2} \right) + \cos\left(\frac{q\pi}{2} - \frac{\epsilon_q \ell_m}{2} \right) \right] \right] \cdot \left[\chi_q \left[J_1(\chi_q R_2) + B_q N_1(\chi_q R_2) \right] - \mathrm{i}\omega\rho_0 Y_{r_q} \left[J_0(\chi_q R_2) + B_q N_0(\chi_q R_2) \right] \right]^{-1} \cdot \frac{\xi_\mu}{\mu^2 - q^2 - q\frac{2\epsilon_q \ell_m}{\pi} - \left(\frac{\epsilon_q \ell_m}{\pi} \right)^2} \right\}. \quad (27)$$

It is worthwhile commenting that the effects of the viscous and thermal phenomena are accounted for in using approximate impedance-like conditions. More sophisticated (non asymptotic) alternative boundary conditions, which respect the fact that viscous and thermal diffusion processes occur near the walls, could equally be chosen, but they would provide the same results because the dimensions of the back-cavity are much greater than the thicknesses of the thermo-viscous boundary layers. Then, viscous and thermal effects play approximately the same role and provide quite the same damping, according to the magnitude of the terms ℓ'_v (viscous effect) and ℓ_h (thermal effect) in expressions (16) and (19).

2.3. Coupled solution for the displacement field of the membrane

Invoking equations (13), (21), (26) and (27), the coefficients ξ_μ (Equation 13) can be expressed in a matrix form as follows:

$$[\xi] = [\eta - \mathbf{I}]^{-1} [\zeta], \quad (28)$$

where

$$\zeta_\mu = \frac{\ell_m}{\pi} \sqrt{\frac{2}{\ell_m}} \frac{1 - (-1)^\mu}{T_z \left[K^2 - k_{z_\mu}^2\right] \mu} p_u, \quad (29)$$

I is the identity matrix, and $[\eta]$ is a square matrix given by

$$\eta_{\mu m} = \sum_{q=0,2,4,\ldots}^{\infty} \frac{\omega^2 \rho_0 \left(\frac{2}{\ell_m}\right) (\nu_q)^2}{T_z \left[K^2 - k_{z_\mu}^2\right]} \frac{L_q}{\chi_q M_q} \frac{\mu \ell_m}{\pi} \cdot \frac{\cos\left(\frac{q\pi}{2} + \frac{\epsilon_q \ell_m}{2}\right) + \cos\left(\frac{q\pi}{2} - \frac{\epsilon_q \ell_m}{2}\right)}{\mu^2 - q^2 - q\frac{2\epsilon_q \ell_m}{\pi} - \left(\frac{\epsilon_q \ell_m}{\pi}\right)^2} \cdot \frac{m\ell_m}{\pi} \frac{\cos\left(\frac{q\pi}{2} + \frac{\epsilon_q \ell_m}{2}\right) + \cos\left(\frac{q\pi}{2} - \frac{\epsilon_q \ell_m}{2}\right)}{m^2 - q^2 - \frac{2q\epsilon_q \ell_m}{\pi} - \left(\frac{\epsilon_q \ell_m}{\pi}\right)^2}, \quad (30)$$

with

$$L_q = J_0(\chi_q R_2) + B_q N_0(\chi_q R_2), \quad (31)$$

and

$$M_q = \left[J_1(\chi_q R_2) + B_q N_1(\chi_q R_2)\right] - \frac{\mathrm{i}\omega\rho_0 Y_{r_q}}{\chi_q} L_q. \quad (32)$$

Finally, the displacement field is expressed as a function of the pressure due to the piezo-electric effect p_u (see Equation 4).

3. Lower order approximation: Equivalent electrical network

When keeping only one mode for the membrane (i.e. $m = \mu = 1$) and only one mode for the cavity (i.e. $q = 0$), the parameters A_q (Equation 27), $\eta_{\mu m}$ (Equation 30), and ζ_μ (Equation 29) become respectively,

$$A_0 = \left[-\omega\rho_0 c_0 2\sqrt{2}/\pi\right] \left[\left[J_1(\chi_0 R_2) + B_0 N_1(\chi_0 R_2)\right] - \mathrm{i}\rho_0 c_0 Y_{r_0}\left[J_0(\chi_0 R_2) + B_0 N_0(\chi_0 R_2)\right]\right]^{-1} \xi_1, \quad (33)$$

$$\eta_{11} = \frac{8}{\pi^2} \frac{\omega\rho_0 c_0}{T_z\left[K^2 - \left(\pi/\ell_m\right)^2\right]} \frac{L_0}{M_0}, \quad (34)$$

and

$$\zeta_1 = \frac{2\ell_m}{\pi}\sqrt{\frac{2}{\ell_m}} \frac{p_u}{T_z\left[K^2 - (\pi/\ell_m)^2\right]}, \quad (35)$$

leading straightforwardly to the expression of the modal expansion coefficient

$$\xi_1 = \frac{2\ell_m}{\pi}\sqrt{\frac{2}{\ell_m}} \frac{p_u}{\frac{8}{\pi^2}\omega\rho_0 c_0 \frac{L_0}{M_0} - T_z\left[K^2 - (\pi/\ell_m)^2\right]}, \quad (36)$$

and to the expression of the average displacement

$$\left\langle \xi(z) \right\rangle_z = \frac{1}{\ell_m}\int_0^{\ell_m} \xi(z)\,\mathrm{d}z = \frac{p_u}{\omega\rho_0 c_0 \frac{L_0}{M_0} - \frac{\pi^2}{8} T_z\left[K^2 - (\pi/\ell_m)^2\right]}. \quad (37)$$

Owing to the expression of the electrical induction D_3 in the radial direction,

$$D_3 = d_{31} T_{\theta\theta} + d_{32} T_{zz} + \varepsilon_{33}^T E_r, \quad (38)$$

the electrical intensity takes the following form

$$I = \mathrm{i}\omega \int_0^{2\pi}\int_0^{\ell_m} D_3\ R_2\,\mathrm{d}z\,\mathrm{d}\theta = \mathrm{i}\omega k_b \left\langle \xi(z) \right\rangle_z + \mathrm{i}\omega\varepsilon_{33}^T(1 - k_{31}^2)\frac{V_r}{t_m} 2\pi R_2 \ell_m, \quad (39)$$

where the electro-mechanical conversion factor k_b is

$$k_b = 2\pi\ell_m \frac{s_{11}^{E^*} d_{31} - s_{12}^{E^*} d_{32}}{s_{E^*}}. \quad (40)$$

Finally, the total impedance of the transducer Z_{T_e} in the electric domain is given by

$$Z_{T_e} = \frac{V_r}{I} = \left[\frac{1}{Z_{E_e}} + \frac{1}{Z_{M_e}} + \frac{1}{Z_{A_e}}\right]^{-1}, \quad (41)$$

where

$$Z_{E_e} = \frac{1}{\mathrm{i}\omega C_e}, \quad (42)$$

is the electrical impedance with

$$C_e = \frac{2\pi R_2 \ell_m}{t_m} \epsilon_{33}^T \left(1 - k_{31}^2\right), \quad (43)$$

where

$$Z_{M_e} = \left(\frac{1}{k_b}\right)^2 \left[\mathrm{i}\omega M_m \frac{\pi^2}{8} + \frac{1}{\mathrm{i}\omega C_m}\frac{\pi^2}{8}\right], \quad (44)$$

the mechanical impedance with

$$M_m = \rho_m t_m S_2, \quad C_m = \frac{1}{S_2}\left[\frac{t_m}{(R_2)^2}\frac{s_{11}^{E^*}}{s_{E^*}} + T_z\left(\frac{\pi}{\ell_m}\right)^2\right]^{-1}, \quad (45)$$

and where

$$Z_{A_e} = \left(\frac{S_2}{k_b}\right)^2 \left[\frac{\pi^2}{8} Z_{\mathrm{rad}} + \frac{k_0}{\mathrm{i}\omega}\frac{\rho_0 c_0^2}{S_2}\frac{L_0}{M_0}\right] \cong \left(\frac{S_2}{k_b}\right)^2 \left[\frac{\pi^2}{8} Z_{\mathrm{rad}} + \frac{1}{\frac{1}{Z_{cav}} + Y_{r_0} S_1 + Y_{r_0} S_2}\right] \quad (46)$$

is the acoustic impedance, L_0 and M_0 being given by equations (31) and (32) respectively, Y_{r_0} by equation (19), and Z_{cav} being expressed as

$$Z_{cav} \cong \frac{\chi_0}{i\omega}\frac{\rho_0 c_0^2}{S_2}\frac{J_0(\chi_0 R_2)}{J_1(\chi_0 R_2)} \cdot \left[1 - \frac{N_1(\chi_0 R_2)}{J_1(\chi_0 R_2)}\frac{J_1(\chi_0 R_1)}{N_1(\chi_0 R_1)}\right]^{-1}, \quad (47)$$

or, in the lowest frequency range,

$$Z_{cav} \cong \frac{1}{\mathrm{i}\omega C_{cav}}, \tag{48}$$

with

$$C_{cav} = \frac{\varrho_m \pi \left(R_2^2 - R_1^2\right)}{\gamma P_0}. \tag{49}$$

It is worth noting that the effects of the thermo-viscous boundary layers at the upper and bottom sides (i.e. at $z = \varrho_m$ and $z = 0$ respectively) of the cavity are taken into account in expression (47), but not in (48). These parameters are represented in the equivalent electrical network given in Figure 4, showing the electrical part, the mechanical part and the acoustical part of the transducer, as well as the conversion factors, where the impedances of the thermal boundary layers $Z_{th}^{(1)}$ and $Z_{th}^{(2)}$ are given by

$$\begin{aligned} Z_{th}^{(1)} &= 1/\left(2\pi R_1 \varrho_m Y_{r_0}\right) \\ \text{and} \quad Z_{th}^{(2)} &= 1/\left(2\pi R_2 \varrho_m Y_{r_0}\right). \end{aligned} \tag{50}$$

4. Experimental and theoretical results

Experimental results obtained for the radiated acoustic pressure are compared in this section to theoretical ones. The measurement of the radiated acoustic pressure has been carried out for two prototypes of emitting transducer, whose dimensions are given in Table I. A $^1/_4$" free-field condenser microphone Brüel & Kjær (B&K) type 4135, with the protecting grid removed, has been used to measure the pressure at a distance of a few centimetres from the transmitter and for $z = \varrho_m/2$. A B&K microphone pre-amplifier type 2669 and a microphone power supply B&K type 2807 have been used for the conditioning of the microphone output signal. A Rohde and Schwarz UPV audio analyser has been used both to supply the electrical voltage to the transmitter, and to compute the Fast Fourier Transforms (FFT) of the measured acoustic pressure. Theoretical results (radiated acoustic pressure) are determined from the complex amplitude $\xi(z)$ of the displacement field of the membrane, which is obtained either from the model presented in Section 2 or from the electrical equivalent network presented in Section 3, using the following expression:

$$p_{\mathrm{rad}}(r, z) = -\frac{\omega \rho_0 c_0}{H_1^{(2)}(k_0 R_2)} H_0^{(2)}(k_0 r)\, \xi(z). \tag{51}$$

This last expression is obtained considering that the cylinder has an infinite length, and using both velocity continuity at $r = R_2$ and the Sommerfeld's radiation condition.

The values of the parameters for the mono-oriented PVDF membrane used for the computation are provided in Table II. Note that the values of the piezoelectric coefficients, the compliance coefficients, the mechanical loss angle, and the permittivity provided by the manufacturer are given for one frequency only (1 kHz or 15 kHz), even though they depend on the frequency. All the values of the parameters for the fluid have been determined considering air at a temperature of 23°C under an atmospheric pressure of 1013.25 hPa and 50% of humidity.

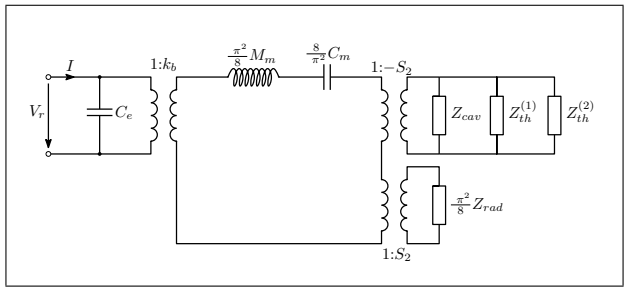

Figure 4. Equivalent electrical circuit of the piezopolymer cylindrical transducer determined from the lower order approximation.

Table I. Dimensions of the two prototypes.

Parameter	Symbol	Prototype A	Prototype B
Inner radius	R_1	1 mm	5 mm
Outer radius	R_2	5 mm	8 mm
Membrane height	ϱ_m	40 mm	30 mm

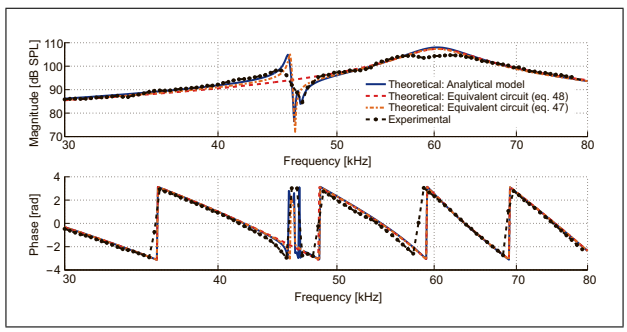

Figure 5. Magnitude (upper graph) [dB SPL] and phase (bottom graph) [rad] of the acoustic pressure radiated by the prototype A as a function of frequency [kHz] at a distance of 2.5 cm and for a peak voltage $V_r = 5$ Vp. Solid line: Theoretical result obtained with the model presented in Section 2 with two modes for the membrane and two axial modes in the cavity. Dashed line: Theoretical result obtained with the equivalent electrical network given in Section 3 when considering very low frequency approximations (Equation 48). Dashed-dotted line: Theoretical result obtained with the equivalent electrical network given in Section 3 when considering low frequency approximations (Equation 47). Solid line with dots: Experimental result.

Figure 5 shows the magnitude and the phase of the pressure emitted by the prototype A, measured at a distance of 2.5 cm, for frequencies between 30 kHz and 80 kHz, and for a supplied peak voltage of 5 Vp. The experimental result is represented by the dashed-line with dots, the theoretical result obtained with the analytical model presented in Section 2 by the solid line, the dashed-line represents the one obtained with the equivalent electrical model

Table II. Values of the parameters for the PVDF membrane.

Parameter	Symbol	Supplier value	Used value	Factor	Units
Membrane thickness	t_m	25	25	$\cdot 10^{-6}$	$[m]$
Membrane density	ρ_m	1.8	1.8	$\cdot 10^{3}$	$[kg/m^3]$
Piezoelectric coefficient	d_{31}	-18	-15	$\cdot 10^{-12}$	$[C/N]$
Piezoelectric coefficient	d_{32}	-3	-3	$\cdot 10^{-12}$	$[C/N]$
Compliance coefficient	s_{11}^E	2.7	2.25	$\cdot 10^{-10}$	$[m^2/N]$
Compliance coefficient	s_{12}^E	-1	-1.25	$\cdot 10^{-10}$	$[m^2/N]$
Mechanical damping	$\tan(\delta_m)$	5	10	$\cdot 10^{-2}$	[-]
Permittivity	ε_{33}^T	1.06	1.06	$\cdot 10^{-10}$	$[F/m]$

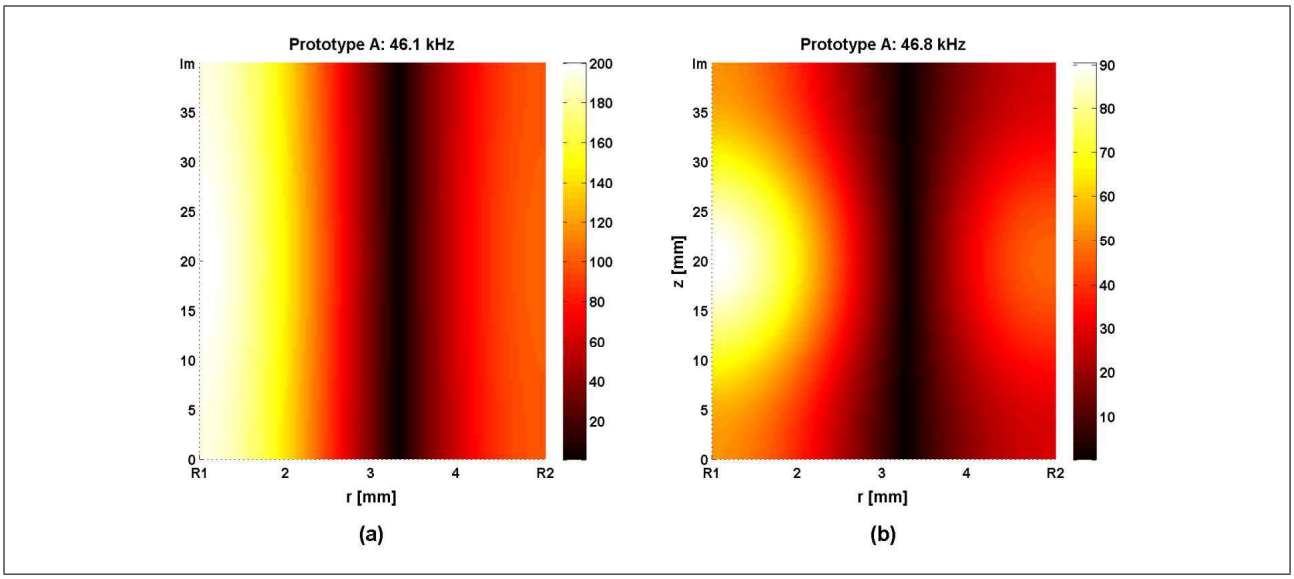

Figure 6. Magnitude [dB SPL] of the theoretical acoustic pressure field (colormap) in the cavity as a function of both the radial (abscissa) and axial (ordinate) coordinates [mm] for prototype A: (a) at 46.1 kHz, and (b) at 46.8 kHz.

(Section 3) when considering approximations in the lowest frequency range of the acoustic impedance of the cavity (Equation 48), and the dashed-dotted line represents the one obtained with the equ ivalent electrical model (Section 3) when considering the less approximated expression of the acoustic impedance of the cavity (Equation 47).

For this prototype, the maximum of pressure amplitude (upper graph) is located at approximately 60 kHz, which corresponds to the first resonance of the membrane given by $1/(2\pi)\sqrt{1/(M_m C_m)}$ (where the mechanical mass M_m and compliance C_m are given by Equation 45). Here, the acoustic load has a negligible effect on the location of this resonance frequency, which depends then on the dimensions and on the characteristics of the PVDF membrane. The resonances and anti-resonances of the system, which are located around 46 kHz, do not appear on the theoretical result obtained with the equivalent electrical network (dashed-line). This is due to the fact that only the first mode is taken into account in this approach (the pressure field in the cavity is assumed to be uniform). Note that when considering expression (47) (instead of Equation 48) in the calculation for the acoustic impedance of the cavity, the pressure is still assumed to be uniform along the z-axis but not any more along the r-axis, and radial mode appear at around 46.1 kHz (dashed-dotted line in Figure 5).

When using the model presented in Section 2 (solid line) and considering two modes for the membrane ($\mu = 1$ & 3 and $m = 1$ & 3) and two axial modes ($q = 0$ & 2) for the pressure field in the cavity, the frequencies of the resonances and anti-resonances of the system are quite well predicted.

The phase of the theoretical radiated pressures in Figure 5 shows a quite good agreement with the experimental one, even around the resonances and anti-resonances of the system located around 46 kHz.

Figure 6a represents the magnitude of the pressure field in the cavity computed using the model presented in section 2 as a function of the radial and axial coordinates at the frequency 46.1 kHz. It shows that the pressure field in the cavity is (quasi) uniform along the axial direction, and that a radial resonance takes place in the cavity. At this frequency, the inner pressure $p_1(R_2, z)$ exerted on the membrane and the displacement field $\xi(z)$ of the membrane are out of phase (close to the opposite-phase), which leads to minimize the amplitude of the displacement field and consequently to minimize the pressure radiated by the transducer. In Figure 5, another anti-resonance of the sys-

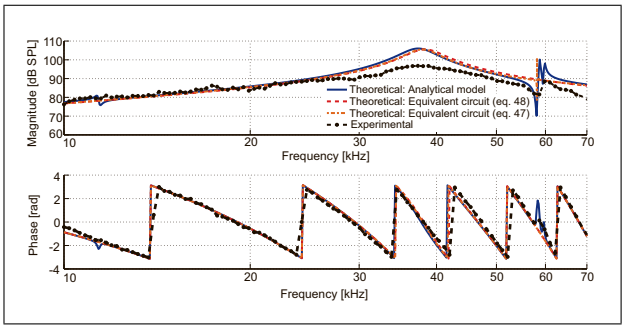

Figure 7. Magnitude (upper graph) [dB SPL] and phase (bottom graph) [rad] of the acoustic pressure radiated by the prototype B as a function of frequency [kHz] at a distance of 3 cm and for a peak voltage $V_r = 4$ Vp. Solid line: Theoretical result obtained with the model presented in section 2 with two modes for the membrane and two axial modes in the cavity. Dashed line: Theoretical result obtained with the equivalent electrical network given in Section 3 when considering very low frequency approximations (Equation 48). Dashed-dotted line: Theoretical result obtained with the equivalent electrical network given in section 3 when considering low frequency approximations (Equation 47). Solid line with dots: Experimental result.

tem appears at approximately 46.8 kHz. As shown in Figure 6b, the magnitude of the pressure field is not uniform along the z-axis, which results from the intricate coupling between the inner pressure and the forced motion of the membrane (forced displacement field).

The discrepancies between theoretical and experimental results may be explained by: 1) the imperfect making of the transducer (rough surface), which can lead to variations in amplitude at some frequencies (such as around 60 kHz), and 2) the use of adhesive-tape to fix the membrane to the discs, which can cause additional damping in the mechanical behavior, and thus reduces the amplitude at the resonances and anti-resonances of the system.

The acoustic pressure emitted by the prototype B, for a supplied peak voltage of 4 Vp, measured at a distance of 3 cm, and for frequencies between 10 kHz and 70 kHz, is shown in Figure 7. At low frequencies, theoretical results fit the experimental one (dotted line with dots). Here, the maximum of pressure amplitude is located around 38 kHz, which corresponds to the first resonance of the membrane given by $1/(2\pi)\sqrt{1/(M_m C_m)}$. It is thought that the differences of amplitude between the theoretical and the experimental results are due to the imperfect making of the transducer, whose membrane surface is not perfectly smooth. For this transducer, the resonances and anti-resonances of the system, due to axial and radial modes, are located around 58 kHz. Theoretical and experimental results show some discrepancies, which may be due to the fact that the mechanical damping involved by the adhesive-tape at the circular boundaries of the membrane is not taken into account in the model (as previously mentioned for the prototype A).

Generally speaking, the pressure radiated by the emitting transducer is essentially governed by the forced motion of the PVDF membrane because the influence of the pressure field inside the cavity plays a weak role, except when resonances due to the coupling between the pressure field in the cavity and the membrane occur. In this last situation, resonances or anti-resonances occur in the acoustic field emitted, depending on the phase between the pressure field behind the membrane and the displacement field of the membrane.

Note that, in the results presented above, the eigenfunction expansions have been evaluated using four terms (the first two modes for both the displacement of the membrane and the axial behaviour of the cavity) because when considering more eigenmodes the results remain practically unchanged.

5. Conclusion

An analytical model for describing a cylindrical emitting transducer, with a PVDF membrane set on a rigid support at its circular edges, has been worked out, which account for the coupled effects between the membrane and its acoustic loads, and the thermo-viscous boundary layer effects in the closed back-cavity. The model is suitable for describing the main properties of the transducers even when considering the low frequency approximations. Therefore, its predictions allow calculating the acoustic field emitted (herein in free space) in a large frequency range (up to 80 kHz).

As a preliminary test of the effectiveness of the model to predict the behavior of the emitted acoustic field as function of the frequency, the analytical results are compared to the experimental ones, with two home-made prototypes. In both cases an overall satisfactory agreement was found between analytical and experimental results, validating the prediction capability of the model.

Nevertheless, minor differences highlighted by this comparison show that the effects of the theoretical dissipative processes are lower than the experimental ones. This could be partly due to an under-evaluation of the mechanical damping but could be essentially due to the defaults of the crudely home-made prototype.

Application might be, for example, in the domain of assistive technologies such as navigation aid glasses or blind sticks for obstacle detection.

Acknowledgements

The authors would like to thank Prof. A.-M. Bruneau for valuable comments, and Garrett Anderson for the corrections of the English text. This publication was supported by the European social fund within the framework of realizing the project “Support of inter-sectoral mobility and quality enhancement of research teams at Czech Technical University in Prague”, CZ.1.07/2.3.00/30.0034.

References

[1] M. Toda: Cylindrical PVDF film transmitters and receivers for air ultrasound. IEEE Trans. Ultrason., Ferroelect., and Freq. Contr. **49** (2002) 626–634.

[2] H. Kawai: The piezoelctricity of poly (vinylidene fluoride). Japan J. Appl. Phys. **8** (1969) 975–976.

[3] Piezo film sensors technical manual. Measurement Specialties, Inc., 1999.

[4] G. Gerliczy, R. Betz: SOLEF®PVDF biaxially oriented piezo- and pyro- electric films for transducers. Sensors and Actuators **12** (1987) 207–223.

[5] M. Tamura, T. Yamaguchi, T. Oyaba, T. Yoshimi: Electroacoustic transducers with piezoelectric high polymer films. J. Audio Eng. Soc. **23** (1975) 21–26.

[6] H. Naono, T. Gotoh, M. Matsumoto, S. Ibaraki, Y. Rikow: Design of an electro-acoustic transducer using piezoelectric polymer film. Audio Eng. Society Convention 58, 1977. Paper Number 1271.

[7] R. Lerch: Electroacoustic transducers using piezoelectric polyvinylidenefluoride films. J. Acoust. Soc. Am. **66** (1979) 952–954.

[8] P. G. Harper, D. M. Treherne, D. Su: A PVDF membrane resonator as a directional acoustic sensor. J. Acoust. Soc. Am. **85** (1989) 468–475.

[9] T. P. Lechner: A velocity microphone using PVF_2 bimorph bending sensors. Acustica **77** (1992) 111–114.

[10] D. Ricketts: Electroacoustic sensitivity of composite piezoelectric polymer cylinders. J. Acoust. Soc. Am. **68** (1980) 1025–1029.

[11] P. Leaver, J. Cunningham, B. E. Jones: Piezoelectric polymer pressure sensors. Sensors and Actuators **12** (1987) 225–233.

[12] A. S. Fiorillo: Design and characterization of a PVDF ultrasonic range sensor. IEEE Trans. Ultrason., Ferroelect., and Freq. Contr. **39** (1992) 688–692.

[13] L. Berquez, V. Haas, J.-L. Franceschi: Détection piézoélectrique en imagerie thermoacoustique (piezoelectric transducer for thermoacoustic imagery). Acta Acust. United Ac. **83** (1997) 868–874.

[14] L. Xiaozhou, Y. Shigong, G. Xiufen, Z. Weiya, L. Rongrong: Study of polymer ultrasonic transducer and complex ultrasonic transducer with PZT/PVDF multi-layer structure. Acta Acust. United Ac. **85** (1999) 420–426.

[15] Q. Mao, S. J. Pietrzko: Measurements of local volume displacement using piezoelectric array. Acta Acust. United Ac. **92** (2006) 556–566.

[16] K. Hatakeyama, S. Kinoshita, A. Haend, T. Asanuma: Development of a loudspeaker system with omni-directional high polymer tweeters. Audio Eng. Society Convention 52, 1975. Paper Number 1056.

[17] B. Locanthi, K. Maekawa, K. Sugano, H. Fukuda, S. Koyano: Development of a loudspeaker system with omnidirectional horn loaded high polymer tweeter. Audio Eng. Society Convention 58, 1977. Paper Number 1302.

[18] R. A. Abram: The theory of a piezoelectric plastic film transducer for earphones. J. Phys. D: Appl. Phys. **13** (1980) 201–207.

[19] G. Davies, P. V. Murphy, G. Maurer: A theoretical and experimental study of a model piezoelectric membrane headphone. J. Acoust. Soc. Am. **76** (1984) 661–665.

[20] Z. Škvor, J. Škvor, Š. Nezbeda: Piezopolymer horn loudspeaker. Audio Eng. Society Convention 102, 1997, 4466–4482.

[21] A. Gallo: For converting between electrical and acoustic energy. Okt. 27 1998. US Patent 5,828,766.

[22] P. Lotton, M. Bruneau, Z. Škvor, A.-M. Bruneau: A model to describe the behaviour of a laterally radiating piezoelectric loudspeaker. Appl. Acoust. **58** (1999) 419–442.

[23] M. Toda, J. Dahl: Phase-matched air ultrasonic transducers using corrugated PVDF film with half wavelength depth. IEEE Trans. Ultrason., Ferroelect., and Freq. Contr. **48** (2001) 1568–1574.

[24] M. Toda, J. Dahl: PVDF corrugated transducer for ultrasonic ranging sensor. Sensors and Actuators A **134** (2007) 427–435.

[25] B. Gazengel, P. Hamery, P. Lotton, A. Ritty: A dome shaped PVDF loudspeaker model. Acta Acust. United Ac. **97** (2011) 800–808.

[26] K. Gürkan, A. Akan: Design of a broadband semi-conical PVDF ultrasonic sensor for obstacle detection applications. 7th International Conference on Electrical and Electronics Engineering (ELECO), 2011, II–333–II–336.

[27] T. Sugimoto, K. Ono, A. Ando, Y. Morita, K. Hosoda, D. Ishii: Semicylindrical acoustic transducer from a dielectric elastomer film with compliant electrodes. J. Acoust. Soc. Am. **130** (2011) 744–752.

[28] G. M. Sessler: Piezoelectricity in polyvinylidenefluoride. J. Acoust. Soc. Am. **70** (1981) 1596–1608.

[29] M. Toda: PVDF cylindrical film air ultrasonic transducer influenced by axial film length. Ultrasonics Symposium, 2014, IEEE, 2014, 1582–1585.

[30] I. Itoh, H. Owada, T. Fujii: Transmitter-receiver of ultrasonic distance measuring device. Apr. 25 1989. US Patent 4,825,116.

[31] M. A. Hersh, M. A. Johnson: Assistive technology for visually impaired and blind people. Springer-Verlag London Limited, 2008.

[32] J. Ealo, A. Jimenez, F. Seco, C. Prieto, J. Roa, F. Ramos, J. Guevara: Broadband omnidirectional ultrasonic transducer for air ultrasound based on EMFi. Ultrasonics Symposium, 2006, IEEE, 2006, 812–815.

[33] M. Toda, S. Tosima: Theory of curved, clamped, piezoelectric film, air-borne transducers. IEEE Trans. Ultrason., Ferroelect., and Freq. Contr. **47** (2000) 1421–1431.

[34] M. Bruneau, T. Scelo (translator and contributor): Fundamentals of acoustics. Wiley-ISTE, 2006.